Multipolar interband absorption in a semiconductor quantum dot. I. Electric quadrupole enhancement

Jorge R. Zurita-Sánchez and Lukas Novotny

The Institute of Optics, University of Rochester, Rochester, New York 14627

Received September 25, 2001; revised manuscript received December 4, 2001

We present a theoretical investigation of a semiconductor quantum dot interacting with a strongly localized optical field as encountered in high-resolution near-field optical microscopy. The strong gradients of these localized fields suggest that higher-order multipolar interactions will affect the standard electric dipole transition rates and selection rules. For a semiconductor quantum dot in the strong confinement limit we calculated the interband electric quadrupole absorption rate and the associated selection rules. We found that the electric quadrupole absorption rate is comparable with the absorption rate calculated in the electric dipole approximation. This implies that near-field optical techniques can extend the range of spectroscopic measurements beyond the standard dipole approximation. However, we also show that spatial resolution cannot be improved by the selective excitation of electric quadrupole transitions. © 2002 Optical Society of America

OCIS codes: 160.4760, 160.6000, 180.5810, 300.6470.

1. INTRODUCTION

Near-field optical techniques have extended the range of optical measurements beyond the diffraction limit and stimulated interest in many disciplines, especially in material sciences and biological sciences.[1,2] The increase of spatial resolution is achieved by access to evanescent modes in the electromagnetic field. These modes are characterized by high spatial frequencies and therefore permit the probing of subwavelength structures. Near-field optical techniques have also been employed for the study of optical properties and dynamics of charge carriers in artificial nanostructures such as quantum wells, quantum wires, and quantum dots (see, for example, Refs. 3–5).

Nanostructures interacting with optical near fields do not necessarily behave in the same way as nanostructures interacting with far-field radiation. For example, as described in Ref. 6, the response of a quantum well when it is excited by the diffracted field of an aperture causes the enhancement of quadrupole transitions, giving rise to a modified absorption spectrum of the quantum well. Furthermore, absorption properties may also be modified as a result of nonlocal spatial dispersion, as described in Ref. 7. Recently Knorr *et al.* formulated a general theoretical, self-consistant multipolar formalism for solids. This formalism can even be extended to account for delocalized charges.[8] The spectral response that originates from the interaction between semiconductor quantum dots and the optical field generated by a small aperture has been discussed in Refs. 9–11. References 10 and 11 account for the highly inhomogeneous excitation field produced by the subwavelength aperture.

In this paper we focus on the interaction of a spherical semiconductor quantum dot with a highly confined optical near field. It has been shown that such fields can be generated near laser-illuminated sharply pointed tips.[12–14] Here we adopt this geometry and approximate the fields near the tip by an oscillating electric dipole oriented along the tip axis. In the research reported in Ref. 15 it was demonstrated that this is a reasonable approximation and that the dipole moment can be related to the computationally determined field enhancement factor. Furthermore, our analysis relies only on the field distribution and does not depend on the actual enhancement factor. We consider here a spherical quantum dot in the strong confinement limit.

The interaction between a quantum dot and the optical near field is described semiclassically by use of the multipolar expansion. For far-field excitation the first term in this expansion, the electric dipole term, gives rise to a response that is considerably stronger than the response produced by subsequent terms. This is so because the physical dimension of the quantum dot is much smaller than the wavelength of optical radiation and is due to the weak spatial variation of the exciting far field. However, the spatial variations of optical near fields are much stronger, and, as consequence, it is suspected that the contribution of higher terms in the multipolar expansion cannot *a priori* be neglected. In this paper we analyze the strength of electric quadrupole absorption compared with the strength of electric dipole absorption. Our study is motivated by a search for the answers to two basic questions: (1) to what extent are standard selection rules modified by higher-order multipolar transitions in confined optical fields and (2) can optical resolution be improved by selective excitation of higher-order multipole transitions. To keep the analysis as simple as possible we neglect Coulomb interaction between hole and electron as well as the spin of these particles.

The paper is organized as follows: The semiclassical multipolar Hamiltonian formalism is presented in Section 2. In the same section we review the wave functions for

the hole and the electron in an ideal spherical quantum dot and outline the field operator representation. In Section 3 we discuss the absorption rate in the electric dipole approximation, and then, in Section 4, derive the absorption rate that arises from the electric quadrupole term in the multipolar expansion. In Section 5 the theory is applied to a quantum dot near a laser-illuminated metal tip. We use approximated parameters for GaAs to estimate the absorption rate for electric dipole transitions and electric quadrupole transitions. Finally, the results are discussed and our conclusions are presented in Section 7.

2. PRELIMINARY CONCEPTS

A. Multipolar Hamiltonian

We use a semiclassical approach to describe the interaction of a quantum dot with the electromagnetic field. In this approach the electromagnetic field obeys Maxwell's equations, and the Hamiltonian of the system ($\hat{H}$) can be separated into two contributions as

$$\hat{H} = \hat{H}_o + \hat{H}_I, \tag{1}$$

where $\hat{H}_o$ and $\hat{H}_I$ are the unperturbed Hamiltonian (absence of fields) and the interaction Hamiltonian, respectively. In the Coulomb gauge they are defined as

$$\hat{H}_o = \frac{1}{2m}\hat{\mathbf{p}}^2 + V(\mathbf{r}), \tag{2}$$

$$\hat{H}_I = -\frac{e}{m}\hat{\mathbf{p}}\cdot\mathbf{A}(\mathbf{r},t) + \frac{e^2}{2m}\mathbf{A}^2(\mathbf{r},t) + e\phi(\mathbf{r},t), \tag{3}$$

where $V(\mathbf{r})$ is the potential energy, $\hat{\mathbf{p}}$ is the canonical momentum, $\mathbf{A}(\mathbf{r},t)$ is the vector potential, and $\phi(\mathbf{r},t)$ is the scalar potential. The multipolar Hamiltonian is obtained by use of canonical transformation $\hat{U} = \exp(iz/\hbar)$, in which z is given by[16,17]

$$z = \int \tilde{\mathbf{P}}(\mathbf{r})\cdot\mathbf{A}(\mathbf{r},t)\mathrm{d}^3r \equiv 0, \tag{4}$$

where $\tilde{\mathbf{P}}(\mathbf{r})$ is the polarization. If vector potential $\mathbf{A}(\mathbf{r},t)$ and scalar potential $\phi(\mathbf{r},t)$ are expanded in a Taylor series with respect to a reference charge distribution at $\mathbf{R}$, as follows:

$$\mathbf{A}(\mathbf{r},t) = \sum_{n=0}^{\infty}\frac{1}{(n+2)n!}[(\mathbf{r}-\mathbf{R})\cdot\nabla]^n\mathbf{B}(\mathbf{R},t) \times(\mathbf{r}-\mathbf{R}), \tag{5}$$

$$\phi(\mathbf{r},t) = \sum_{n=0}^{\infty}\frac{-1}{(n+1)!}(\mathbf{r}-\mathbf{R})[(\mathbf{r}-\mathbf{R})\cdot\nabla]^n\cdot\mathbf{E}(\mathbf{R},t), \tag{6}$$

then this choice of $\mathbf{A}(\mathbf{r},t)$ and $\phi(\mathbf{r},t)$ satisfies condition (4). By substituting Eqs. (5) and (6) into Eq. (3) we obtain

$$\hat{H}_I = \hat{H}^E + \hat{H}^M + \hat{H}^Q + \ldots. \tag{7}$$

Here $\hat{H}^E$, $\hat{H}^M$, and $\hat{H}^Q$ are the first three terms of the multipolar expansion, namely, the electric dipole, the magnetic dipole, and the electric quadrupole, respectively, which are defined as

$$\hat{H}^E = -\mathbf{d}\cdot\mathbf{E}(\mathbf{r},t)|_{\mathbf{r}=\mathbf{R}}, \tag{8a}$$

$$\hat{H}^M = -\mathbf{m}\cdot\mathbf{B}(\mathbf{r},t)|_{\mathbf{r}=\mathbf{R}}, \tag{8b}$$

$$\hat{H}^Q = -\nabla_1\cdot\tilde{\mathbf{Q}}\mathbf{E}(\mathbf{r}_1,t)|_{\mathbf{r}_1=\mathbf{R}}. \tag{8c}$$

$\mathbf{d}$, $\mathbf{m}$, and $\tilde{\mathbf{Q}}$ are the electric dipole moment, the magnetic dipole moment, and the electric quadrupole moment, respectively, with respect to a reference charge distribution at $\mathbf{R}$. Nabla operator ∇_1 acts only on the spatial coordinates $\mathbf{r}_1$ of the electric field. It is important to mention that $\mathbf{m}$ depends on the canonical momentum. However, for weak fields the canonical momentum can be approximated as the mechanical momentum.

B. Quantum Dot Wave Functions (Strong Confinement)

We assume that a spherical quantum dot is made from a direct bandgap semiconductor for which the bulk electric dipole transitions are allowed between the valence band and the conduction band. In a generic manner we assume that the valence band has a p-like character and that the conduction band has an s-like character. The latter assumption is commonly encountered for several semiconductors such as GaAs. We also assume that an electron and a hole are completely confined in a sphere with radius a by the potential energy

$$V(r) = \begin{cases} 0 & r \leqslant a \\ \infty & r > a \end{cases}, \tag{9}$$

where r is the radial coordinate. Also, we assume that the electron (hole) has the same effective mass m_e (m_h) as in the bulk material. This assumption is valid if the volume of the sphere is much larger than the volume of a primitive cell in the crystal. Strong confinement is achieved if the Bohr radii of electron b_e and hole b_h are much larger than the radius of the quantum dot, a. By assuming the aforementioned conditions we can express the wave function of the electron in the conduction band as

$$\Psi^e(\mathbf{r}) = \frac{1}{\sqrt{V_o}}u_{c,0}(\mathbf{r})\zeta^e(\mathbf{r}). \tag{10}$$

Here $u_{c,0}(\mathbf{r})$ is the conduction band Bloch function (with lattice periodicity) that has the corresponding eigenvalue $k = 0$, and V_o is the volume of the unit cell. Similarily, the corresponding wave function for the hole in the valence band is

$$\Psi^h(\mathbf{r}) = \frac{1}{\sqrt{V_o}}u_{v,0}(\mathbf{r})\zeta^h(\mathbf{r}), \tag{11}$$

where $u_{v,0}(\mathbf{r})$ is the valence band Bloch function with eigenvalue $k = 0$. $\zeta^e(\mathbf{r})$ and $\zeta^h(\mathbf{r})$ are the envelope functions, which vary spatially much more slowly than $u_{v,0}(\mathbf{r})$ and $u_{c,0}(\mathbf{r})$. Roughly, the energy difference between adjacent electron (hole) energy levels is $(\hbar^2/m_e a^2)$ $[\hbar^2/(m_h a^2)]$. If this energy difference is much larger

than Coulomb interaction $e^2/(4\pi\varepsilon_o\epsilon a^2)$, the electron–hole interaction can be neglected. Under this assumption, envelope function $\zeta^{e(h)}(\mathbf{r})$ for the electron (hole) satisfies the time-independent Schrödinger equation in which the potential energy is given by Eq. (9). The solution in spherical coordinates $(r,\ \theta,\ \phi)$ is given by

$$\zeta^{e(h)}_{n,l,m}(r,\ \theta,\ \phi) = \Lambda_{nl}(r)Y_{l,m}(\theta,\ \phi). \tag{12}$$

Here $Y_{l,m}(\theta,\ \phi)$ are the spherical harmonics, and the radial function $\Lambda_{nl}(r)$ is

$$\Lambda_{nl}(r) = \sqrt{\frac{2}{a^3}}\frac{1}{j_{l+1}(\beta_{nl})}j_l\left(\beta_{nl}\frac{r}{a}\right). \tag{13}$$

j_l is the lth-order spherical Bessel function and β_{nl} is the nth root of j_l, that is, $j_l(\beta_{nl}) = 0$. The corresponding energy levels $\mathcal{E}^{e,h}$ are found to be

$$\mathcal{E}^e = \mathcal{E}_g + \frac{\hbar^2}{2m_e}\left(\frac{\beta_{nl}}{a}\right)^2, \tag{14}$$

$$\mathcal{E}^h = \frac{\hbar^2}{2m_h}\left(\frac{\beta_{nl}}{a}\right)^2, \tag{15}$$

where $\mathcal{E}_g$ is the bulk energy bandgap. Figure 1 shows the resultant level scheme. According to Eqs. (14) and (15) the energy is independent of quantum number m; thus energy level nl is $(2l + 1)$-fold degenerate.

C. Field Operator Representation

The annihilation carrier field operator $\{\hat{\Psi}\}$ can be expressed as a linear combination of hole creation operators in the valence band and electron annihilation operators in the conduction band, that is,[18,19]

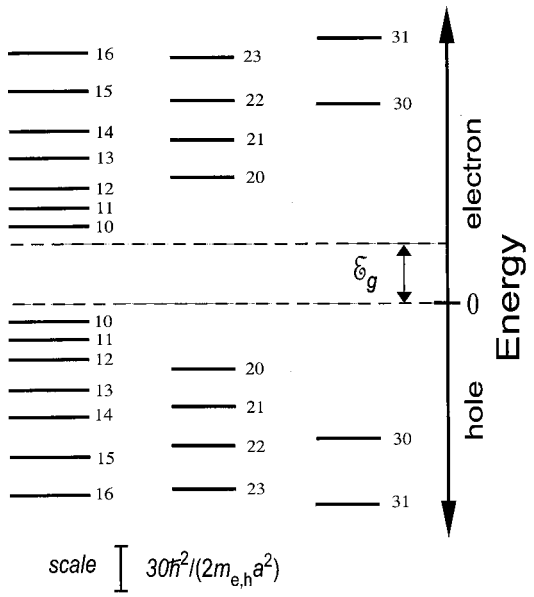

Fig. 1. Energy-level diagram of a spherical quantum dot according to Eqs. (14) and (15). Each energy level is characterized by quantum numbers n and l, and its degeneracy corresponds to quantum number m. Differently from the case of a hydrogen atom, quantum number n does not restrict the number of suborbitals l.

$$\hat{\Psi}(\mathbf{r}) = \sum_{n,l,m}\left[\frac{1}{\sqrt{V_o}}u_{c,0}(\mathbf{r})\zeta^e_{nlm}(\mathbf{r})\hat{f}_{nlm} + \frac{1}{\sqrt{V_o}}u_{v,0}(\mathbf{r})\zeta^h_{nlm}(\mathbf{r})\hat{g}^\dagger_{nlm}\right]. \tag{16}$$

$\hat{f}_{nlm}$ is the annihilation operator for an electron in the conduction band with envelope function $\zeta^e_{nlm}(\mathbf{r})$; $\hat{g}^\dagger_{nlm}$ is the creation operator for a hole in the valence band with envelope function $\zeta^h_{nlm}(\mathbf{r})$. Creation carrier field operator $\hat{\Psi}^\dagger$ is the adjoint of Eq. (16).

3. ABSORPTION IN THE ELECTRIC DIPOLE APPROXIMATION

We consider a monochromatic electric field oscillating with frequency ω as

$$\mathbf{E}(\mathbf{r},\ t) = \tilde{\mathbf{E}}(\mathbf{r})\exp(-i\omega t) + \text{c.c.} \tag{17}$$

Here $\tilde{\mathbf{E}}(\mathbf{r})$ is the spatial complex amplitude and c.c. means a complex conjugate. By setting origin O at the center of the quantum dot and using the rotating-wave approximation we arrive at an electric dipole transition rate α^E for photon absorption[18,19]:

$$\alpha^E = K_e\sum_{nml}\sum_{rst}\tilde{\delta}_{nr}\tilde{\delta}_{ls}\tilde{\delta}_{mt}\delta[\hbar\omega - (\mathcal{E}^e_{nl} + \mathcal{E}^h_{rs})], \tag{18}$$

where $\tilde{\delta}$ is the Kronecker delta tensor, δ is the Dirac delta function, and K_e is the absorption strength, given by

$$K_e = \frac{2\pi}{\hbar}e^2|\tilde{\mathbf{E}}(\mathbf{0})\cdot\mathbf{P}_{cv}|^2, \tag{19}$$

$$\mathbf{P}_{cv} = \frac{1}{V_o}\int_{\text{UC}}u^*_{c,0}(\mathbf{r}')\mathbf{r}'u_{v,0}(\mathbf{r}')\mathrm{d}^3r' = -\frac{\hbar}{m_o\omega}\mathbf{m}_{cv}. \tag{20}$$

Here $\mathbf{m}_{cv}$ is defined as

$$\mathbf{m}_{cv} \equiv \frac{1}{V_0}\int_{\text{UC}}u^*_{c,0}(\mathbf{r}')\nabla' u_{v,0}(\mathbf{r}')\mathrm{d}^3r', \tag{21}$$

where UC denotes the volume of the unit cell. In Eq. (20) we have used the fact that $\hat{\mathbf{r}} \equiv -i\hat{\mathbf{p}}/m_o\omega$ (m_o and e are the rest mass and the charge of the electron, respectively). From Eq. (18) we notice that the absorption strength (K_e) depends only on the bulk material properties of the quantum dot. That is, it depends on Bloch functions u_{c0} and u_{v0}, and it is not influenced by the envelope functions $\zeta^{e,h}_{nlm}(\mathbf{r})$. Also, Eq. (18) indicates that the allowed transitions are those for which electron and hole have the same quantum numbers, that is,

$$n = r, \qquad l = s, \qquad m = t.$$

These relationships define the selection rules for electric dipole transitions in a semiconductor quantum dot.

4. ABSORPTION ARISING FROM THE QUADRUPOLE TERM

A. Electric Quadrupole Hamiltonian

The electric quadrupole interaction Hamiltonian $\hat{H}^Q$ can be represented as

$$\hat{H}^Q = \int \hat{\Psi}^\dagger(\mathbf{r}) H^Q(\mathbf{r}) \hat{\Psi}(\mathbf{r}) \mathrm{d}^3 r, \tag{22}$$

$$H^Q(\mathbf{r}) = -\nabla_1 \cdot \vec{\mathbf{Q}}(\mathbf{r}) \mathbf{E}(\mathbf{r}_1, t)|_{\mathbf{r}_1=0}, \tag{23}$$

where the $\vec{\mathbf{Q}}(\mathbf{r})$ is the quadrupole moment:

$$\vec{\mathbf{Q}}(\mathbf{r}) = (1/2) e \mathbf{r}\mathbf{r}. \tag{24}$$

Here and in what follows, the subsequent listing of two vectors [as in Eq. (24)] denotes the outer product (dyadic product). The interband terms are found by substitution of Eq. (16) and its adjoint into Eq. (22), thus:

$$\hat{H}^Q = -\nabla_1 \cdot \left[\sum_{nlm} \sum_{rst} \hat{f}^\dagger_{nlm} \hat{g}^\dagger_{rst} \int u^*_{c,0}(\mathbf{r}) \zeta^{e*}_{nlm}(\mathbf{r}) \times \vec{\mathbf{Q}}(\mathbf{r}) u_{v,0}(\mathbf{r}) \zeta^h_{rst}(\mathbf{r}) \mathrm{d}^3 r \right] \mathbf{E}(\mathbf{r}_1, t) \Big|_{\mathbf{r}_1=0} + \text{h.c.}, \tag{25}$$

where (h.c.) denotes the Hermitian conjugate. We calculate the integral on the right-hand side of Eq. (25) by decomposing it into a sum of integrals over the volume occupied by each of the unit cells. Applying the coordinate transformation $\mathbf{r}' = \mathbf{r} - \mathbf{R}_q$, where $\mathbf{R}_q$ is a translational lattice vector (the lattice remains unchanged when it is translated by $\mathbf{R}_q$), yields for Eq. (25)

$$\hat{H}^Q = -\nabla_1 \cdot \left[e \sum_{nlm} \sum_{rst} \sum_q \hat{f}^\dagger_{nlm} \hat{g}^\dagger_{rst} \int_{\mathrm{UC}} u^*_{c,0}(\mathbf{r}' + \mathbf{R}_q) \times \zeta^{e*}_{nlm}(\mathbf{r}' + \mathbf{R}_q) \vec{\mathbf{Q}}(\mathbf{r}' + \mathbf{R}_q) u_{v,0}(\mathbf{r}' + \mathbf{R}_q) \times \zeta^h_{rst}(\mathbf{r}' + \mathbf{R}_q) \mathrm{d}^3 r' \right] \mathbf{E}(\mathbf{r}_1, t) \Big|_{\mathbf{r}_1=0} + \text{h.c.} \tag{26}$$

Because $u_{i,0}(\mathbf{r}' + \mathbf{R}_q) = u_{i,0}(\mathbf{r}')$ $(i = c, v)$ and the functions $\zeta^h_{nlm}(\mathbf{r}' + \mathbf{R}_q)$ and $\zeta^e_{nlm}(\mathbf{r}' + \mathbf{R}_q)$ are practically constant in each unit cell volume, Eq. (26) can be approximated as

$$\hat{H}^Q \approx -\nabla_1 \cdot \left[e \sum_{nlm} \sum_{rst} \sum_q \hat{f}^\dagger_{nlm} \hat{g}^\dagger_{rst} \zeta^{e*}_{nlm}(\mathbf{R}_q) \zeta^h_{rst}(\mathbf{R}_q) \times (\tfrac{1}{2} \mathbf{R}_q \mathbf{P}_{cv} + \tfrac{1}{2} \mathbf{P}_{cv} \mathbf{R}_q + \vec{\mathbf{Q}}_{cv}) \right] \mathbf{E}(\mathbf{r}_1, t) \Big|_{\mathbf{r}_1=0} + \text{h.c.} \tag{27}$$

Here $\mathbf{P}_{cv}$ is given by Eq. (20) and $\vec{\mathbf{Q}}_{cv}$ is defined as

$$\vec{\mathbf{Q}}_{cv} = \frac{1}{2V_o} \int_{\mathrm{UC}} u^*_{c,0}(\mathbf{r}') \mathbf{r}' \mathbf{r}' u_{v,0}(\mathbf{r}') \mathrm{d}^3 r'. \tag{28}$$

The term containing $\mathbf{R}_q \mathbf{R}_q$ has vanished because of the orthogonality of the Bloch functions, i.e., $\langle u_{i,0} | u_{j,0} \rangle = \tilde{\delta}_{ij}$; $i, j = c, v$. $\vec{\mathbf{Q}}_{cv}$ vanishes because we are assuming that the valence band is p like and the conduction band is s like. Thus, using $\vec{\mathbf{Q}}_{cv} = 0$ and replacing $\Sigma_q \to \int \mathrm{d}R$ yield for relation (27)

$$\hat{H}^Q = -\nabla_1 \cdot \left[e \sum_{nlm} \sum_{rst} \hat{f}^\dagger \hat{g}^\dagger [\tfrac{1}{2} \mathbf{P}_{cv} \mathbf{D}_{nmlrst} + \tfrac{1}{2} \mathbf{D}_{nmlrst} \mathbf{P}_{cv}] \right] \mathbf{E}(\mathbf{r}_1, t)|_{\mathbf{r}_1=0} + \text{h.c.} \tag{29}$$

Here $\mathbf{D}_{nmlrst}$ is defined as

$$\mathbf{D}_{nmlrst} \equiv \int \zeta^{e*}_{nlm}(\mathbf{R}) \mathbf{R} \zeta^h_{rst}(\mathbf{R}) \mathrm{d}^3 R, \tag{30}$$

with the integration running over the volume of the quantum dot. Equation (29) is the final expression for electric quadrupole Hamiltonian $\hat{H}^Q$. The factor $\mathbf{D}_{nmlrst}$ depends only on the envelope functions. Using the definition of $\zeta^{e,h}_{nlm}(\mathbf{R})$ given by Eq. (12) yields for $\mathbf{D}_{nmlrst}$

$$\begin{aligned} \mathbf{D}_{nmlrst} = A_{nlrs} B_{lm} B_{st} \Bigg(& \frac{C_{st}}{2(2l+1)} (\mathbf{n}_x \pm i \mathbf{n}_y) \\ & \times \{ \tilde{\delta}_{(m+1)t} [\tilde{\delta}_{l(s-1)} + \tilde{\delta}_{l(s+1)}] \\ & + \tilde{\delta}_{(m-1)t} [(l-m+1)(l-m+2) \tilde{\delta}_{l(s-1)} \\ & - (1+m)(l+m-1) \tilde{\delta}_{l(s+1)}] \} \\ & + \mathbf{n}_z C_{lm} \tilde{\delta}_{mt} \left[\frac{l+m+1}{2l+3} \tilde{\delta}_{l(s-1)} + \frac{l-m}{2l-1} \tilde{\delta}_{l(s+1)} \right] \Bigg), \end{aligned} \tag{31}$$

where $\mathbf{n}_x$, $\mathbf{n}_y$, and $\mathbf{n}_z$ are the Cartesian unitary vectors, and the coefficients A_{nlrs}, B_{lm}, and C_{lm} are given by

$$A_{nlrs} \equiv 2\pi \int_0^a R^3 \Lambda_{nl}(R) \Lambda_{rs}(R) \mathrm{d}R, \tag{32a}$$

$$B_{lm} \equiv \left[\frac{(2l+1)}{4\pi} \frac{(l-m)!}{(l+m)!} \right]^{1/2}, \tag{32b}$$

$$C_{lm} \equiv \frac{2(l+m)!}{(2l+1)(l-m)!}. \tag{32c}$$

B. Electric Quadrupole Selection Rules and Absorption Rate

Using the Fermi Golden Rule yields the electric quadrupole transition rate (α^Q) for photon absorption:

$$\alpha^Q = \frac{2\pi}{\hbar} \sum_{nlm} \sum_{rst} |\langle nml; rst | \hat{H}^Q_{\mathrm{int}} | 0 \rangle|^2 \delta[\hbar\omega - (\mathcal{E}^e_{nl} + \mathcal{E}^h_{rs})]. \tag{33}$$

Here $|0\rangle$ is the ground state of the quantum dot. By substituting Eq. (29) into Eq. (33) we obtain the electric quadrupole transition rate:

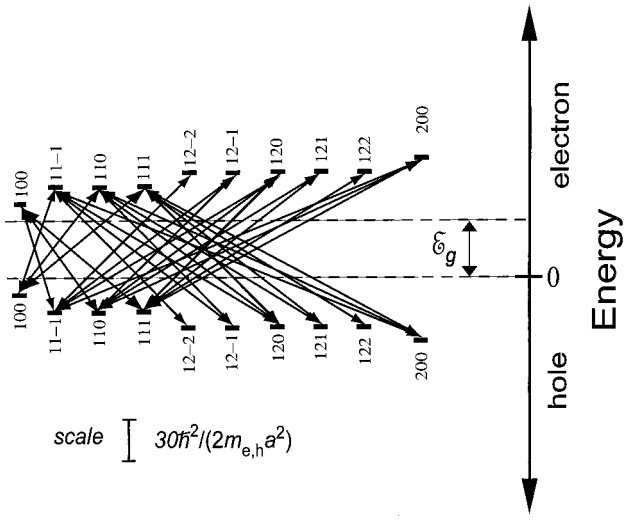

Fig. 2. Diagram of the allowed electric quadrupole transitions in a spherical quantum dot. The energy levels are labeled by the quantum numbers *nlm* (electron) and *rst* (hole). The selection rules are [$l - s = \pm 1$ and ($m - t = \pm 1$ or $m - t = 0$)]. The allowed electric quadrupole transitions exclude the allowed electric dipole transitions.

$$\alpha^Q = \frac{2\pi}{\hbar} e^2 \sum_{nlm} \sum_{rst} |\nabla_1 \cdot (\tfrac{1}{2}\mathbf{P}_{cv}\mathbf{D}_{nmlrst} + \tfrac{1}{2}\mathbf{D}_{nmlrst}\mathbf{P}_{cv})\tilde{\mathbf{E}}(\mathbf{r}_1)|_{\mathbf{r}_1=0}|^2 \delta[\hbar\omega - (\mathcal{E}^e_{nl} + \mathcal{E}^h_{rs})]. \tag{34}$$

We find that the electric quadrupole absorption rate contains the dyadic product of $\mathbf{P}_{cv}$ and $\mathbf{D}_{nmlrst}$ and vice versa. Whereas $\mathbf{P}_{cv}$ depends on the bulk material properties, $\mathbf{D}_{nmlrst}$ depends on the quantum dot properties [see Eqs. (20) and (31)]. This term implies that the allowed electric quadrupole transitions occur when the quantum numbers l, s, m, and t fulfill

$$m - t = \pm 1, \qquad l - s = \pm 1$$

or

$$m - t = 0, \qquad l - s = \pm 1.$$

These relationships form the selection rules for the electric quadrupole transitions in a semiconductor quantum dot. Figure 2 illustrates the first few allowed quadrupole transitions. We find that the quadrupole selection rules exclude any electric dipole allowed transitions and therefore allow us to separate the electric quadrupole transitions spectroscopically from the electric dipole transitions.

5. ABSORPTION RATES IN STRONGLY CONFINED OPTICAL FIELDS

To compare the electric dipole and the electric quadrupole absorption rates in strongly confined optical fields we consider a quantum dot in the vicinity of a laser-illuminated metal tip. This situation is encountered in so-called apertureless schemes of near-field optical microscopy. The strongest light confinement is achieved when the metal tip is irradiated with light polarized along the tip's axis. For this situation Fig. 3(a) shows field distribution ($|\mathbf{E}|^2$) rigorously calculated by the multiple multipole method[20] near a gold tip with a 10-nm end diameter and irradiated with $\lambda = 800$-nm light.[21] In the multiple multipole method, electromagnetic fields are represented by a series expansion of known analytical solutions of Maxwell's equations. To determine the unknown coefficients in the series expansion we impose boundary conditions at discrete points on the interfaces between adjacent homogeneous domains. The calculated field distribution for our particular geometry can be well approximated by the field generated by an electric dipole aligned along tip axis z and located at the origin of tip curvature. Figure 3(b) demonstrates the validity of this dipole approximation: rigorously calculated field strength ($|\mathbf{E}|^2$) for the metal tip is plotted along the z axis (solid curve) and compared with the corresponding field generated by the dipole (dashed curve).[15] The only adjustable parameter is dipole moment $\mathbf{p}_o$, which can be related to the computationally determined field enhancement factor. Because of this very good approximation, we simply replace the laser-illuminated metal tip with a dipole.

Electric field $\mathbf{E}(\mathbf{r})$ generated by an oscillating electric dipole with moment $\mathbf{p}_o$ located at $\mathbf{r}_o$ and oscillating at angular frequency ω can be represented as

$$\tilde{\mathbf{E}}(\mathbf{r}) = \frac{k_o^2}{\varepsilon_o} \overleftrightarrow{\mathbf{G}}(\mathbf{r}, \mathbf{r}_o, \omega)\mathbf{p}_o. \tag{35}$$

Here $k_o = \omega/c$, where c is the vacuum speed of light, and $\overleftrightarrow{\mathbf{G}}(\mathbf{r}, \mathbf{r}_o, \omega)$ is the free-space dyadic Green's function.[22] We consider the situation depicted in Fig. 4 for which a sharp metal tip illuminated with light polarized along the tip's axis (z axis) is replaced by a dipole with magnitude p_o and oriented in the z direction. The dipole is located at $\mathbf{r}_o = z_o\mathbf{n}_z$, and the quantum dot coordinates are $\mathbf{r} = x\mathbf{n}_x + y\mathbf{n}_y$. The quantum dot is scanned in the plane $z = 0$ while the position of the exciting dipole is kept fixed.

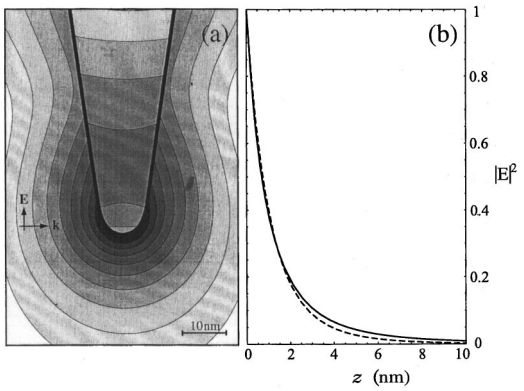

Fig. 3. (a) Computed field distribution ($|\mathbf{E}|^2$) near a gold tip irradiated by a plane wave polarized along the tip's axis. Logarithmic scaling with a factor of 2 between successive contour lines. (b) Comparison of the computed field ($|\mathbf{E}|^2$, solid curve) with the corresponding field of a dipole ($|\mathbf{E}|^2$, dashed curve) oriented along the tip's axis and located inside the tip. Both fields are evaluated along tip axis z, where $z = 0$ coincides with the tip's surface.

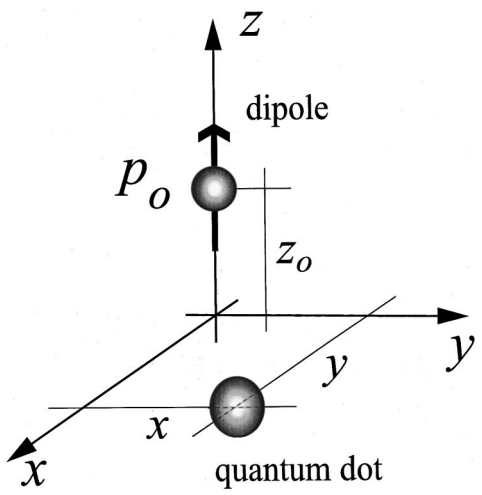

Fig. 4. Simplified configuration of a quantum dot ($\mathbf{r} = x\mathbf{n}_x + y\mathbf{n}_y$) interacting with a laser-illuminated metal tip. The tip is replaced with a vertical dipole ($\mathbf{r}_o = z_o\mathbf{n}_z$) with moment p_o and oriented along the z axis.

To calculate electric quadrupole absorption rate (α^Q) and electric dipole absorption rate (α^E) we consider Bloch functions for the valence band and the conduction band that are similar to those of GaAs. If we ignore spin–orbit coupling and spin degeneracy, the p-like valence band is threefold degenerate. The Bloch functions are calculated by the empirical pseudo-potential method with parameters taken from Ref. 23. GaAs has a lattice constant of $d = 0.565$ nm, and the effective masses of electron and hole are $m_e = 0.067m_o$ and $m_h = 0.080m_o$ (light hole), respectively. Inclusion of the heavy hole will shift the hole energy levels only as long as the heavy-hole Bohr radius is larger than the quantum dot radius.

We consider the lowest allowed electric dipole transition, i.e., the transition with the lowest allowed energy difference between initial and final states. During this transition an electron with quantum numbers (100) and a hole with quantum numbers (100) are created. As there is no preferential coordinate axis we take the rotational average of Eq. (18). Also, taking into account the degeneracy of the valence band (threefold) yields as the averaged electric dipole absorption rate

$$\langle \alpha^E \rangle = \langle K_e \rangle \delta[\hbar\omega - (\mathcal{E}^e_{10} + \mathcal{E}^h_{10})], \tag{36}$$

where $\langle K_e \rangle$ is

$$\langle K_e \rangle = \frac{2\pi}{\hbar} e^2 |\tilde{\mathbf{E}}(0)|^2 |\mathbf{P}|^2 \tag{37}$$

and

$$|\mathbf{P}| = |\mathbf{P}_{cv_1}| = |\mathbf{P}_{cv_2}| = |\mathbf{P}_{cv_3}|. \tag{38}$$

By computing numerically the integral of Eq. (20) over a unit cell of the crystal we obtain that $|\mathbf{P}| \approx 0.75d$.

The lowest energy allowed electric quadrupole transition creates a hole with quantum numbers (110), (11-1), or (111) (threefold degeneracy) and an electron with quantum numbers (100). Again, there is no preferential coordinate axis, so the rotational average of Eq. (34) has to be evaluated. Because the electric quadrupole moment is the dyadic product of two vectors with independent orientations, the rotational average of Eq. (34) is obtained in a straightforward manner. After the average is evaluated and the degeneracy of the valence band and the hole energy level are taken into account, the averaged electric quadrupole absorption rate becomes

$$\langle \alpha^Q \rangle = \langle K^Q \rangle \delta[\hbar\omega - (\mathcal{E}^e_{10} + \mathcal{E}^h_{10})]. \tag{39}$$

Here $\langle K^Q \rangle$ corresponds to

$$\langle K^Q \rangle = \frac{2\pi}{\hbar} \frac{e^2}{2} |\mathbf{P}|^2 |\mathbf{D}|^2 \times \sum_{i,j} \left[\left| \frac{\partial}{\partial x_i} \tilde{E}_j(\mathbf{0}) \right|^2 + \frac{\partial}{\partial x_i} \tilde{E}_j(\mathbf{0}) \frac{\partial}{\partial x_j} \tilde{E}^*_i(\mathbf{0}) \right]. \tag{40}$$

The ith Cartesian coordinate is denoted x_i, and $\tilde{E}_i(\mathbf{r})$ is the ith Cartesian component of the electric field $\tilde{\mathbf{E}}_i(\mathbf{r})$. $|\mathbf{D}|$ corresponds to

$$|\mathbf{D}| = |\mathbf{D}_{100110}| = |\mathbf{D}_{100111}| = |\mathbf{D}_{10011-1}|. \tag{41}$$

The integration of Eq. (41) over the quantum dot volume renders a value $|\mathbf{D}| \approx 0.3a$.

6. DISCUSSION OF THE NEAR-FIELD–QUANTUM DOT INTERACTION

We analyze absorption rates for quantum dots with the two different radii, $a = 5$ nm and $a = 10$ nm. For $a = 5$ nm the electric quadrupole transition is excited at a wavelength of $\lambda \approx 500$ nm; the electric dipole transition, at $\lambda \approx 550$ nm. The quadrupole transition for a quantum dot of radius $a = 10$ nm occurs at $\lambda \approx 615$ nm, and the electric dipole transition at $\lambda \approx 630$ nm.

For a quantum dot that is just beneath the exciting dipole ($\mathbf{r} = \mathbf{0}$), Figure 5 shows the ratio of the quadrupole absorption rate and the dipole absorption rate ($\langle \alpha^Q \rangle / \langle \alpha^E \rangle$) as a function of normalized separation z_o/λ. The vertical dashed lines indicate the minimum physical distance between the quantum dot and the dipole, i.e., the limit at which the tip and the quantum dot would touch (we assume a tip radius of 5 nm).

For the quantum dot with radius $a = 5$ nm and an excitation wavelength of $\lambda = 550$ nm the normalized minimum distance is $z_o{}^{\min}/\lambda \approx 0.018$. Similarly, for the quantum dot with radius $a = 10$ nm and a wavelength of $\lambda = 630$ nm the minimum distance is 15 nm, which corresponds to a normalized distance of $z_o{}^{\min}/\lambda \approx 0.024$. The important finding is that the ratio $\langle \alpha^Q \rangle / \langle \alpha^E \rangle$ can be as high as 0.3 for a 5-nm quantum dot [see Fig. 5(a)] and even 0.6 for a 10-nm quantum dot [see Fig. 5(b)]. These values are roughly 3 orders of magnitude larger than those obtained by use of far-field excitation [for plane-wave excitation the ratio is of the order of $(a/\lambda)^2$]. Thus we find that, in the extreme near field ($z_o < \lambda/10$), quadrupole transitions become important and the electric dipole approximation is not sufficiently accurate.

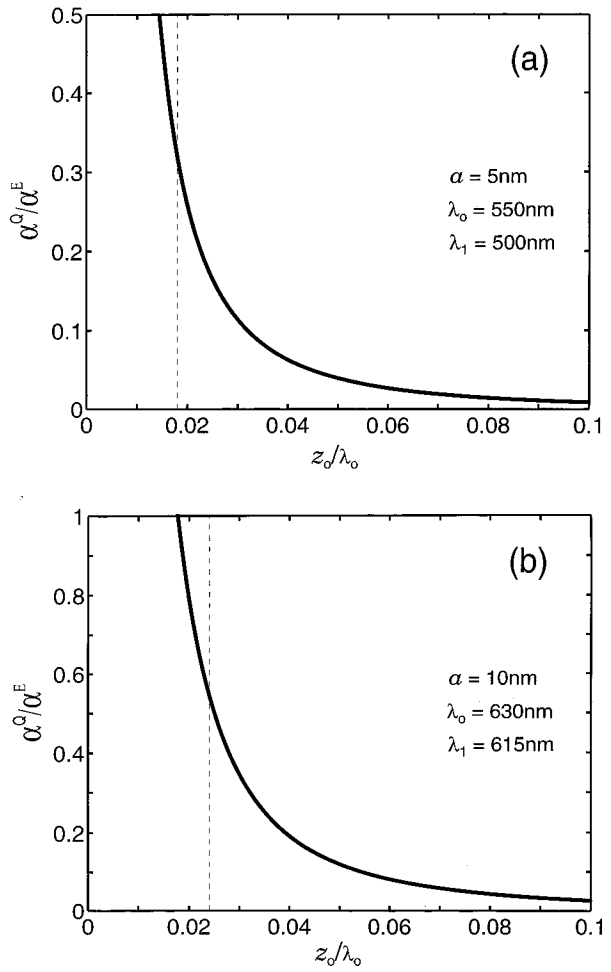

Fig. 5. Ratio of electric quadrupole absorption rate $\langle \alpha^Q \rangle$ and electric dipole absorption rate $\langle \alpha^E \rangle$ as a function of normalized distance (z_o/λ_o) between excitation dipole ($\mathbf{r}_o = z_o \mathbf{n}_z$) and quantum dot center ($\mathbf{r} = \mathbf{0}$). The quantum dot radius is (a) $a = 5$ nm and (b) $a = 10$ nm. Vertical dashed lines: minimum physical separation between the center of the quantum dot and the exciting dipole. This separation corresponds to $a_t + a$, where $a_t = 5$ nm is the radius of curvature of the metal tip.

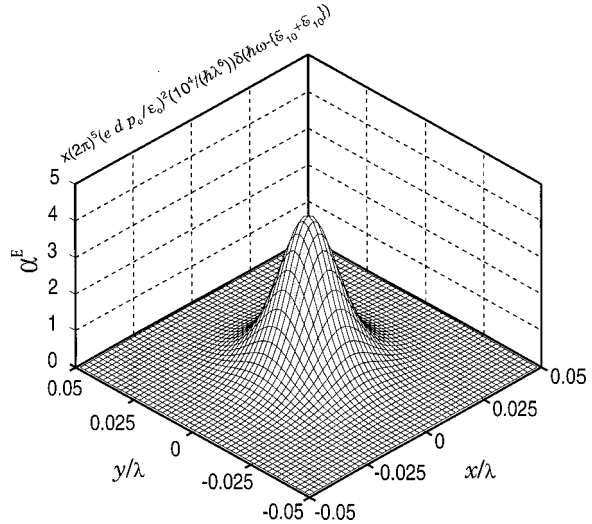

Fig. 6. Electric dipole absorption rate $\langle \alpha^E \rangle$ as a function of normalized lateral coordinates $(x/\lambda, y/\lambda)$. The height of the excitation dipole is $z_o = 0.025\lambda$. e, d, and p_o denote the elementary charge, the lattice constant, and the dipole moment, respectively.

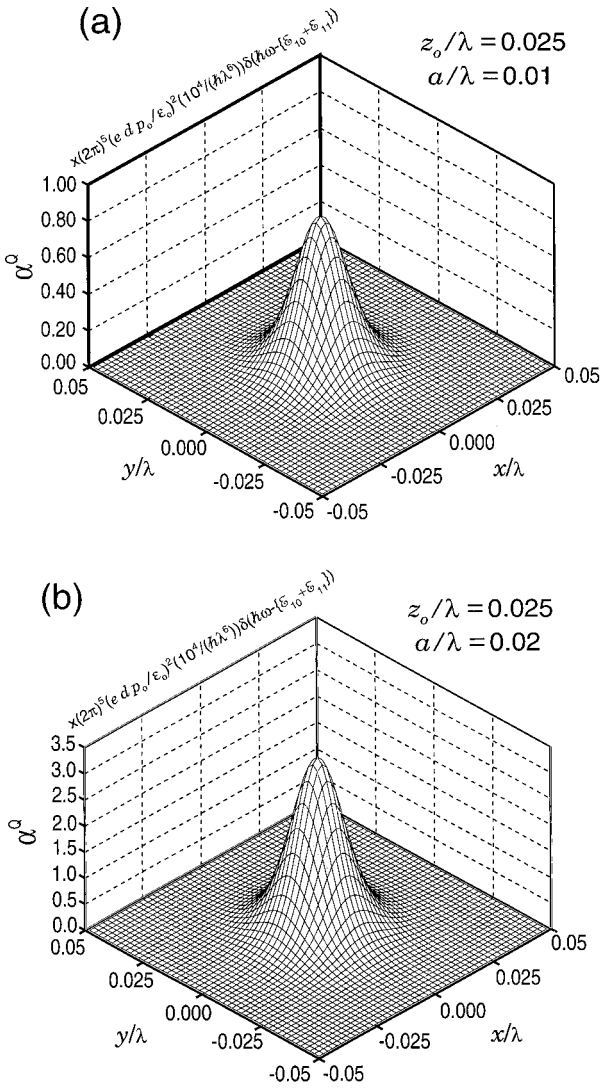

Fig. 7. Electric dipole absorption rate $\langle \alpha^Q \rangle$ as a function of normalized lateral coordinates $(x/\lambda, y/\lambda)$. The height of the excitation dipole is $z_o = 0.025\lambda$. e, d, and p_o denote the elementary charge, the lattice constant, and the dipole moment, respectively. The quantum dot radius is (a) $a = 0.01\lambda$ and (b) $a = 0.02\lambda$. The width of the curve is roughly the same as in Fig. 6, which indicates that no improvement of resolution can be achieved by quadrupole transitions.

We generated the plots in Figs. 6 and 7 by scanning the quantum dot in the xy plane while keeping the exciting dipole at constant height z_o. Figure 6 shows the electric dipole absorption rate $\langle \alpha^E \rangle$, whereas Fig. 7 shows the electric quadrupole absorption rate $\langle \alpha^Q \rangle$. Both plots are symmetrical with respect to the z axis. For $\langle \alpha^E \rangle$ this symmetry is generated by the dominant field component $\tilde{E}_z$, whereas for $\langle \alpha^Q \rangle$ the symmetry is due to the strong field gradient $\partial \tilde{E}_z / \partial z$. The electric dipole absorption rate is proportional to the square of the particle dipole moment p_o and to the square of the lattice constant of the crystal d. The quadrupole absorption rate is also proportional to the square of (a/λ), as is evident from Fig. 7, where the ratio a/λ in Fig. 7(b) is twice the ratio a/λ in Fig. 7(a). A comparison of the widths of the curves in Figs. 6 and 7 shows that no improvement of spatial reso-

lution can be achieved by selective probing of optical quadrupole transitions.

7. CONCLUSIONS

We have analyzed higher-order multipole interactions between a semiconductor quantum dot and a strongly confined optical field. Expressions have been derived for the electric quadrupole interaction Hamiltonian, the associated absorption rate, and selection rules. It has been assumed that the quantum dot has a p-like valence band and an s-like conduction band. Also, the Bohr radii of electron and hole were assumed to be larger than the sphere radius (strong confinement limit), and no Coulomb interactions between hole and electron have been taken into account. Because they have different selection rules, electric dipole and electric quadrupole interband transitions can be separated and selectively excited. The electric quadrupole absorption strength depends on the bulk properties of the material (Bloch functions) as well as on the envelope functions (confinement functions). In this way it differs from the electric dipole absorption strength, which depends only on the bulk properties of the semiconductor. When the quantum dot with radius a interacts with the confined optical field produced by a sharply pointed tip, the ratio between the electric quadrupole absorption rate and the electric dipole absorption rate can be as high as 0.3 for $a = 5$ nm and even 0.6 for $a = 10$ nm. Electric quadrupole transitions cannot be ignored in the extreme near field, i.e., for separations between tip and quantum dot smaller than $\lambda/10$. The inclusion of electric quadrupole transitions modifies the absorption spectra of quantum dots in the extreme near field. However, we have shown that no improvement in spatial resolution can be achieved by selective probing of electric quadrupole transitions. Future studies will be directed at electric quadrupole excitonic interactions.

ACKNOWLEDGMENTS

We thank Stephan W. Koch and Andreas Knorr for valuable input to this study. This research was supported by the U.S. Department of Energy through grant DE-FG02-01ER15204 and by a Fulbright–Consejo Nacional de Ciencia y Tecnología fellowship for J. R. Zurita-Sánchez.

REFERENCES

1. For a recent review, see, R. C. Dunn, "Near-field scanning optical microscopy," Chem. Rev. **99**, 2891–2927 (1999).
2. N. van Hulst, ed., *Proceedings of the 6th International Near-field Optics Conference*, J. Microsc. (Oxford) **202**, 1–450 (2001).
3. R. D. Grober, T. D. Harris, J. K. Trautman, E. Betzig, W. Wegscheider, L. Pfeiffer, and K. W. West, "Optical spectroscopy of GaAs/AlGaAs quantum wire structure using near-field scanning optical microscopy," Appl. Phys. Lett. **64**, 1421–1423 (1994).
4. J. Levy, V. Nikitin, J. M. Kikkawa, A. Cohen, N. Samarth, R. Garcia, and D. D. Awschalom, "Spatiotemporal near-field spin microscopy in patterned magnetic heterostructures," Phys. Rev. Lett. **76**, 1948–1951 (1996).
5. A. Richter, M. Stüptitz, Ch. Lienau, T. Elsaesser, M. Ramsteiner, R. Nötzel, and K. H. Ploog, "Carrier trapping into single GaAs quantum wires studied by variable temperature near-field spectroscopy," Ultramicroscopy **71**, 205–212 (1998).
6. A. von der Heydt, A. Knorr, B. Hanewinkel, and S. W. Koch, "Optical near-field excitation at the semiconductor band edge: field distributions, anisotropic transitions and quadrupole enhancement," J. Chem. Phys. **112**, 7831–7838 (2000).
7. O. Mauritz, G. Goldoni, F. Rossi, and E. Molinari, "Local optical spectroscopy in quantum confined systems: a theoretical description," Phys. Rev. Lett. **82**, 847–850 (1999).
8. A. Knorr, S. W. Koch, and W. W. Chow, "Optics in the multipole approximation: from atomic systems to solids," Opt. Commun. **179**, 167–178 (2000).
9. B. Hanewinkel, A. Knorr, P. Thomas, and S. W. Koch, "Optical near-field response of semiconductor quantum dots," Phys. Rev. B **55**, 13,715–13,725 (1997).
10. G. W. Bryant, "Probing quantum nanostructures with near-field microscopy and vice versa," Appl. Phys. Lett. **72**, 768–770 (1998).
11. A. Chavez-Pirson and S. T. Chu, "A full vector analysis of near-field luminescence probing of a single quantum dot," Appl. Phys. Lett. **74**, 1507–1509 (1999).
12. H. F. Hamann, M. Kuno, A. Gallagher, and D. J. Nesbitt, "Molecular fluorescence in the vicinity of a nanoscopic probe," J. Chem. Phys. **114**, 8596–8609 (2001).
13. Y. C. Martin, H. F. Hamann, and H. K. Wickramasinghe, "Strength of the electric field in apertureless optical near-field microscopy," J. Appl. Phys. **89**, 5774–5778 (2001).
14. E. J. Sánchez, L. Novotny, and X. S. Xie, "Near-field fluorescence microscopy based on two-photon excitation with metal tips," Phys. Rev. Lett. **82**, 4014–4017 (1999), and references therein.
15. L. Novotny, "Forces in optical near-fields," in *Near-Field Optics and Surface Plasmon Polaritons*, S. Kawata, ed. (Springer-Verlag, Berlin, 2001), pp. 123–141.
16. R. G. Woolley, "A comment on 'The multiple Hamiltonian for time dependent fields,' " J. Phys. B **6**, L97–L99 (1973).
17. L. D. Barron and C. G. Gray, "The multiple interaction Hamiltonian for time dependent fields," J. Phys. A **6**, 59–61 (1973).
18. H. Haug and S. W. Koch, *Quantum Theory of the Optical and Electronic Properties of Semiconductors* (World Scientific, Singapore, 1993).
19. L. Bányai and S. W. Koch, *Semiconductor Quantum Dots* (World Scientific, Singapore, 1993).
20. Ch. Hafner, *The Generalized Multiple Multipole Technique for Computational Electromagnetics* (Artech House, Norwood, Mass., 1990).
21. L. Novotny, R. X. Bian, and X. S. Xie, "Theory of nanometric optical tweezers," Phys. Rev. Lett. **79**, 645–648 (1997).
22. C. T. Tai, *Dyadic Green's Functions in Electromagnetic Theory* (Institute of Electrical and Electronics Engineers, Piscataway, N.J., 1993).
23. P. Yu and M. Cardona, *Fundamentals of Semiconductors* (Springer-Verlag, Berlin, 1996).